Available online at www.sciencedirect.com

SCIENCE DIRECT®

Remote Sensing of Environment 92 (2004) 397–408

Remote Sensing of Environment

www.elsevier.com/locate/rse

Comparison of AVIRIS and Landsat ETM+ detection capabilities for burn severity

Jan W. van Wagtendonk[a,*], Ralph R. Root[b], Carl H. Key[c]

[a] USGS Western Ecological Research Center, Yosemite Field Station, 5083 Foresta Road, El Portal, CA 95318, USA
[b] USGS Rocky Mountain Mapping Center, Denver, CO 80225, USA
[c] USGS Northern Rocky Mountain Science Center, West Glacier, MT 55936, USA

Received 19 June 2003; received in revised form 12 November 2003; accepted 18 December 2003

Abstract

Our study compares data on burn severity collected from multi-temporal Airborne Visible and Infrared Imaging Spectrometer (AVIRIS) with similar data from the Enhanced Thematic Mapper Plus (ETM+) using the differenced Normalized Burn Ratio (dNBR). Two AVIRIS and ETM+ data acquisitions recorded surface conditions immediately before the Hoover Fire began to spread rapidly and again the following year. Data were validated with 63 field plots using the Composite Burn Index (CBI). The relationship between spectral channels and burn severity was examined by comparing pre- and post-fire datasets. Based on the high burn severity comparison, AVIRIS channels 47 and 60 at wavelengths of 788 and 913 nm showed the greatest negative response to fire. Post-fire reflectance values decreased the most on average at those wavelengths, while channel 210 at 2370 nm showed the greatest positive response on average. Fire increased reflectance the most at that wavelength over the entire measured spectral range. Furthermore, channel 210 at 2370 nm exhibited the greatest variation in spectral response, suggesting potentially high information content for fire severity. Based on general remote sensing principles and the logic of variable spectral responses to fire, dNBR from both sensors should produce useful results in quantifying burn severity. The results verify the band–response relationships to burn severity as seen with ETM+ data and confirm the relationships by way of a distinctly different sensor system.
Published by Elsevier Inc.

Keywords: Burn severity; AVIRIS; Multi-temporal; Landsat ETM+; Yosemite National Park

1. Introduction

Throughout the world, large fires in recent years have increased the need for information about burned areas in order for land managers to assess the impacts of fires on landscapes. Required levels of information are often difficult to obtain, however, especially where fire size, remoteness, and rugged terrain impede direct observation of burned areas. Thus, managers increasingly must turn to remote sensing technologies to extend knowledge and to quantify the extent and severity of fires.

Remote sensing has been used for many years to assess burn scars on several continents. For example, in Europe Koutsias et al. (1999) reported on programs designed to map burned areas on a local scale, and Chuvieco (1999) used several indices to measure changes in the vegetation mosaic resulting from a large fire on the Mediterranean coast of Spain. Efforts in Asia have focused on mapping burned areas in Siberia (Bourgeau-Chaves et al., 2002) and in Indonesia (Siegert & Ruecker, 2000). The amount of biomass burned by fires in southern Africa was mapped by Eva and Lambin (1998), and Scholes et al. (1996) used the Along Track Scanning Radiometer (ATSR) to map burned areas in central Africa.

The Advanced Very High Resolution Radiometer (AVHRR) was used in South America by Hlavka et al. (1996) to map fire scars in the Brazilian Cerrodo. In Northern Australia, SPOT-VEGETATION imagery has been used to detect burned areas (Stroppiana et al., 2002). North America applications have included locating and estimating the size of fires in Alaska (Boles & Verbyla, 1999; Kasischke & French, 1995) and mapping boreal forest fires in Canada (Li et al., 2000).

Although maps and estimates of burned area are of critical importance to land managers, information about the

* Corresponding author. Tel.: +1-209-379-1306; fax: +1-209-379-1116.
E-mail address: jan_van_wagtendonk@usgs.gov (J.W. van Wagtendonk).

0034-4257/$ - see front matter. Published by Elsevier Inc.
doi:10.1016/j.rse.2003.12.015

heterogeneity of burn severity patterns within the perimeter of a fire is equally valuable. Severity is defined as the degree to which a site has been altered by fire (National Wildfire Coordinating Group, 1996). As such, it is a measure of the magnitude of the effect that the fire has on the environment and is commonly applied to a number of ecosystem components. Although both fire line intensity and burning duration affect the level of severity, their combined effect can vary. Furthermore, the same fire behavior can result in different severity effects to the soils, understory vegetation and overstory vegetation. While post-fire effects can be observed immediately after a fire, burn severity takes a year to several years before becoming evident. Remote sensing of burn severity has not been applied as widely as fire detection and burned area analyses.

Traditional methods for detecting burn severity have concentrated on evaluating post-fire Multispectral Scanner (MSS), Thematic Mapper (TM), and Enhanced Thematic Mapper Plus (ETM+) scenes for vegetation regeneration using Normalized Difference Vegetation Index (NDVI) values. For example, Diaz-Delgado et al. (2003) used a temporal sequence of NDVI values from TM and MSS images to map severity levels for a large fire in Spain. They compared their results to a fire severity map derived from field measurements of burned shrubs (Perez & Moreno, 1998). In the USA, severity detection was improved over NDVI when a single post-fire TM band 7 scene was used (White et al., 1996). However, without multi-temporal differencing, burned area was not always discernable from unburned background, and the scale of band 7 reflectance was not necessarily related to the magnitude of change due to fire.

Methods similar to the NDVI have been used to detect changes in leaf water content. Hunt and Rock (1989) developed the Normalized Difference Infrared Index calculated from the difference between ratios of reflectance values at 820 and 1600 nm. They concluded that indices derived from near infrared and mid-infrared reflectances were not sensitive enough to remotely sense water stress. Gao (1996) calculated the Normalized Difference Water Index (NDWI) from the difference between ratios of reflectance values at 860 and 1240 nm. He tested the NDWI using Airborne Visible and Infrared Imaging Spectrometer (AVIRIS) data and found the NDWI useful for remote sensing of vegetation liquid water.

In order to assist management of fire-scarred landscapes, Patterson and Yool (1998) used a single post-fire TM scene for mapping vegetation mortality. They compared the Kauth–Thomas and principal component analysis transformation techniques and found acceptable results if the data have sufficient spatial, radiometric, and spatial resolutions. Similarly, Kushlaw and Ripple (1998) evaluated TM data to map forest survival after a wildland fire in Oregon, USA. Regressions of single-date TM band transformations accounted for 73% of the variation of post-fire canopy, while stratification by pre-fire tasseled cap wetness explained 78%. Miller and Yool (2002) explored the use of multi-temporal TM and ETM+ data for assessing appropriate post-fire watershed treatments and minimizing subsequent erosion effects. Their analysis included an algorithm contrasting bands 4 and 7 for detecting canopy consumption after the Cerro Grande Fire in New Mexico. When compared to canopy consumption classification made by field crews, their three-class supervised classification yielded a kappa of 0.86.

TM data have been used to calculate a radiometric index of burn severity called the Normalized Burn Ratio, or NBR (Key & Benson, 1999, 2002; Key et al., 2002). Multi-temporal differencing was employed to enhance contrast and detection of changes from pre- to post-fire using Landsat TM bands 4 and 7. The temporal difference between the pre- and post-fire NBR values is called the differenced Normalized Burn Ratio (dNBR). This difference is hypothesized to represent optimal separation of burned area from unburned surroundings and to provide a scaled index of the magnitude of change caused by fire, hence the burn severity. The dNBR is now widely used by land managers in the USA to assess landscape-level fire severity (Lutes et al., in press). Coupled with a standard field measure of burn severity called the Composite Burn Index (CBI) developed by Key and Benson (2004), the dNBR provides an accurate, repeatable detection of burn severity.

While these techniques have proven useful, it is possible that higher spatial and spectral resolution could provide greater insight into the impact of severity on vegetation resources. Moreover, hyperspectral data, such as provided by AVIRIS, may be used to validate assumptions about the response sensitivity of Landsat bandwidths to burn severity. AVIRIS data have been used to map chaparral fuels in California (Roberts et al., 1998) and New Mexico (Morath & Rockwell, 2002). The AVIRIS and Hymap sensors have been used to assess burned area extent in New Mexico and Wyoming, respectively (Morath & Rockwell, 2002). After the Yellowstone fires in 1988, Kokaly (2002) was able to use AVIRIS imagery to map forest cover types and forest recovery. Riano et al. (2002) assessed vegetation regeneration post-fire with multi-temporal AVIRIS images using NDVI; however, no attempts have been made to assess severity using imaging spectroscopy for calculating dNBR with pre- and post-fire imagery.

The objective of this study was to determine whether the dNBR calculated from Landsat ETM+ data provides optimum signals of burn severity, as validated independently by AVIRIS; and if AVIRIS could more accurately portray burn severity than data collected from the ETM+ sensor. This opportunity arose in Yosemite National Park, USA, when AVIRIS imagery was reflown in consecutive years before and after a large lightning-caused fire was allowed to burn under prescribed conditions.

2. Study area

Yosemite National Park is a 300,000-ha reserve in the Sierra Nevada of California, USA (Fig. 1). Elevations range from 600 m in the foothills to 4000 m at the crest. The park has a moderate climate with hot, dry summers and cold, moist winters. Temperatures range from a mean minimum of −11 °C in January at the high elevations to a mean maximum of 32 °C in July at the lower elevations. Normal annual precipitation also varies with elevation from 80 cm on the western boundary to a maximum of 122 cm at the med-elevations, most of it as snow.

The vegetation responds to climate and topography with chaparral woodlands in the foothills, conifer forests covering the montane and subalpine zones, and alpine meadows above tree line. The dry chaparral woodlands consist of manzanita (*Arctostaphylos viscida*) and ceanothus (*Ceanothus cuneatus*) underneath canyon and interior live oaks (*Quercus chrysolepsis* and *Quercus wislizenii*) and foothill pine (*Pinus sabiniana*). As elevation increases, pure ponderosa pine (*Pinus ponderosa*) stands become mixed with incense-cedar (*Calocedrus decurrens*), sugar pine (*P. lambertiana*), California black oak (*Quercus kelloggii*), and increasing amounts of white fir (*Abies concolor*). This mixture gives way to nearly pure red fir (*Abies magnifica*) forests with western white pine (*Pinus monticola*), western juniper (*Juniperus occidentalis*), and Jeffrey pine (*Pinus jeffrey*) occurring on exposed granitic ridges. The subalpine forest is dominated by lodgepole pine (*Pinus contorta*), which, as treeline, is approached is replaced by mountain hemlock (*Tsuga mertensiana*) and whitebark pine (*Pinus albicaulis*). Meadows consisting of herbs, grasses, sedges, and shrubs occur at all elevations.

Lightning strikes are pervasive in the park and ignite numerous fires each year (van Wagtendonk et al., 2002). Fire plays a natural role in all the vegetation zones except

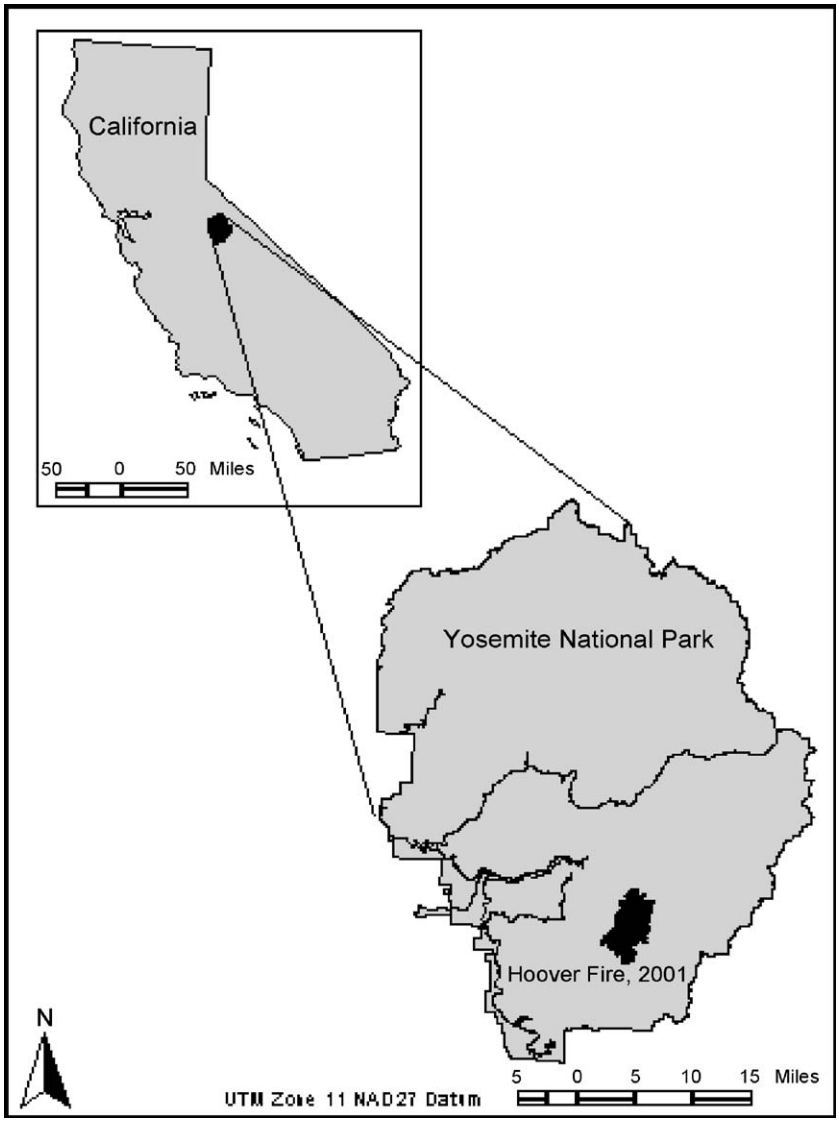

Fig. 1. Location of the Hoover Fire in Yosemite National Park, California, USA.

the alpine zone. The park has had an active fire management program for over 30 years, initiating prescribed burning in 1970 and allowing wildland fires to burn under prescribed conditions since 1972. The Hoover Fire was ignited by lightning on July 26, 2001, in the Illilouette Creek drainage south of Yosemite Valley (Fig. 1). The fire spread slowly until August 18, when it expanded rapidly with increasing winds. By October 22, 2001, when it was extinguished by snow, the fire had burned 2961 ha.

3. Methods

The National Park Service, in conjunction with the U.S. Geological Survey, initiates a burn severity assessment on all fires greater than 40 ha that occur in national parks. For the Hoover Fire, Landsat ETM+ scenes from pre- and post-fire acquisitions were processed through the burn severity mapping program at the USGS Eros Data Center (Key et al., 2002). The scenes from July 27, 2000, and August 2, 2002, respectively, were terrain corrected and transformed to reflectance before computing the NBR for each scene:

$$\mathrm{NBR}_{\mathrm{ETM+}} = 1000[(R_4 - R_7)/(R_4 + R_7)],$$

where R values are per-pixel reflectance calculated for bands 4 and 7, respectively, using the radiance and reflectance equations given by Markham and Barker (1986). The dNBR was then calculated by subtracting the post-fire NBR from the pre-fire NBR:

$$\mathrm{dNBR}_{\mathrm{ETM+}} = \mathrm{NBR}_{\mathrm{pre}} - \mathrm{NBR}_{\mathrm{post}}$$

During September 2002, field crews established a total of 63 CBI plots in high severity, moderate severity, low severity, and unburned areas. Plot locations were selected from a random sample of homogeneous areas within $\mathrm{dNBR}_{\mathrm{ETM+}}$ strata defined by Key and Benson (2004). High severity areas were typified by near complete combustion of all of the litter, duff, and small logs, the mortality of small to medium sized trees, and the consumption of the crowns of large trees (Fig. 2). Moderate severity stands retained some fuels on the forest floor, although there was mortality of small trees and scorching of the crowns of medium and large sized trees (Fig. 3), while low severity stands were generally lightly burned with only the fine fuels removed and some scorching of the understory trees (Fig. 4). Unburned stands had accumulations of woody and litter fuels, thick understories of trees, and low live branches (Fig. 5).

Severity was interpreted as the degree of environmental change on a site, using the CBI. The CBI aggregated multiple rating factors within multiple strata of the community to derive a summary severity value over a 30-m diameter plot (Key & Benson, 2004). Rating factors included the amounts of altered and unaltered vegetation, the degree of resprouting from vegetation that burned, the consumption or charring of substrate materials, and the amount of newly exposed mineral soil, among others. The strata consisted of substrates, low vegetation less than 1 m high, taller shrubs and sapling trees up to 7 m tall, intermediate-sized trees, and big trees. The CBI provided a continuous scale of severity between 0.0 and 3.0 for the understory, overstory, and total plot. Those values were correlated with the scanner-derived indices to explore degrees of association between burn severity and changes in spectral reflectance. The mean dNBR values for five points including the plot center and four points 14 m from the center were used in regressions with the CBI values.

Fig. 2. High severity stands within the Hoover Fire, September 2002. Most of the litter, duff, and small logs are consumed and few needles remain in the crowns.

Coincident with effort to assess burn severity using ETM+ imagery, a project to map fuel characteristics throughout Yosemite with AVIRIS imagery was being conducted. The AVIRIS sensor delivers calibrated images of the spectral radiance in 224 contiguous spectral channels with wavelengths from 400 to 2500 nm (Green et al., 1998). The first AVIRIS data acquisition recorded surface conditions on August 17, 2001, the day before the fire's rapid spread (Flight f010817t01). Since clouds obscured some areas of the park and the sensor's cooling system malfunctioned during one flight line, the park was reflown 1 year later on July 22, 2002 (Flight f020722t01). The two flights provided the opportunity to compare burn severity assessments between data collected by the ETM+ sensor and by the AVIRIS sensor.

Both AVIRIS flights were with the NASA ER-2 jet flying at approximately 16.7 km above sea level, at about 730 km/hr. Seven flight lines oriented in a north–south direction were required to cover the park each year, with flight lines 4 and 5 encompassing the burned area. In 2001,

Fig. 3. Moderate severity stands within the Hoover Fire, September 2002. Litter and duff are reduced and scorched needles are present in the crowns.

flight line 4 was over the fire at 2027 h GMT with a solar zenith angle of 64.68° and an azimuth angle of 127.29°. For flight line 5, the time was 2042 h GMT, the zenith angle was 20.14°, and the solar angle was 122.27°. In 2002, flight line 4 was above the fire at 1840 h GMT with the solar angle of 39.05° and an azimuth of 104.36°. The time for flight line 5 was 1829 GMT; the solar angle was 37.03°; and the solar azimuth was 102.54°.

Fig. 4. Low severity stands within the Hoover Fire, September 2002. There is spotty reduction of litter, duff, and small branch wood, and the crowns contain both green and scorched needles.

Fig. 5. Unburned stands within the Hoover Fire, September 2002. These stands have accumulations of litter, duff, and woody debris, and the green crowns reach the forest floor.

The AVIRIS data were fully orthorectified via a pixel-by-pixel ray tracing from the sensor focal point to the USGS-supplied DEM according to a locally optimized camera model (Boardman, personal communication). The model accounted for the scan geometry, optic and sensor arrays. Aircraft ephemeris data (time, latitude, longitude, altitude, roll, pitch, heading) were recorded in-flight. Ground control points were used to bootstrap a parametric adjustment to the ephemeris to account for systematic errors in the data and model.

The data were calibrated to reflectance and corrected for atmospheric moisture using the ACORN algorithm. To derive the NBR_{AVIRIS}, only one channel per complementary ETM+ bandwidth was selected, choosing the ones showing most change, and not averaging all applicable channels across the bandwidths. This selection isolated the most responsive AVIRIS channels to see how NBR_{AVIRIS} compared to the NBR_{ETM+}. The NBR was calculated for each scene and a dNBR calculated for the entire fire using AVIRIS channels 47 and 210:

$$NBR_{AVIRIS} = 1000[(R_{47} - R_{210})/(R_{47} + R_{210})].$$

The relationship between spectral channels and burn severity was examined by differencing pre- and post-fire datasets:

$$dNBR_{AVIRIS} = NBR_{pre} - NBR_{post}$$

The per-channel reflectance differences quantified the spectral response over the time interval and indicated the

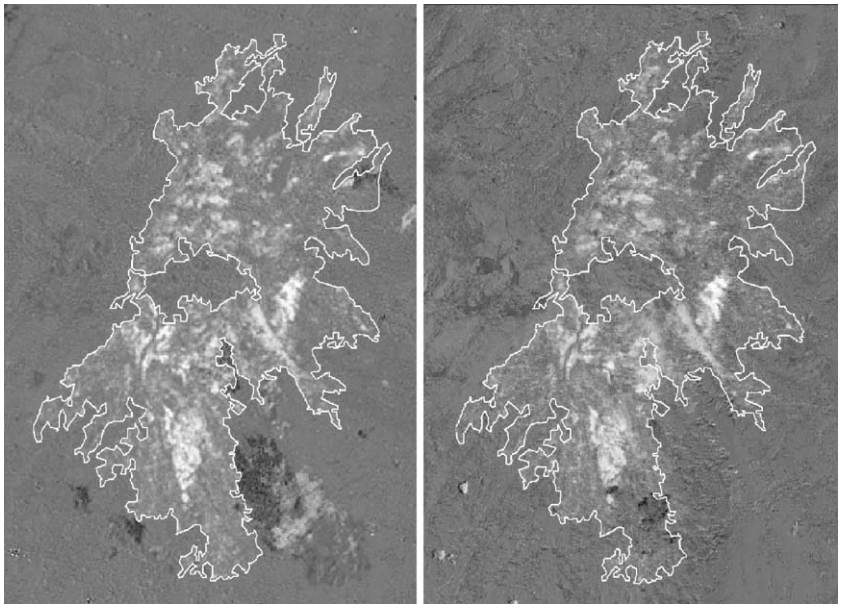

Fig. 6. The dNBR for the Hoover burn area, ETM+ on the left and AVIRIS on the right. The gray scale indicates the magnitude of change in NBR. Neutral or very little change as medium gray predominates outside the burn.

degree of spectral change due to the fire. Temporal response in apparent reflectance was measured from pre- to post-fire for high severity, moderate severity, low severity, and unburned areas. The designation of within-burn severity level was generalized into three broadly characterized regions spanning the full range of apparent fire effects. Ranges of apparent fire effects were determined by post fire reconnaissance, and the within-burn pixel frequency distribution for $dNBR_{ETM+}$. The distribution was simply divided into the three severity regions, solely for the purpose of grouping pixels for comparison, and not as a rigorous a priori definition of the severity.

4. Results

The dNBR results from both sensors exhibited very similar patterns in terms of both spatial distribution and degree of change due to fire (Fig. 6). Post-fire clouds in the ETM+ scene minimally affected areas within the burn but did not impact sample locations. While the burn did not encompass very large uniform patches of any particular level of severity, the exhibited spatial complexity provided a good test of sensor capability. Moreover, a gradient from very low to high degree of change was evident and was sufficiently distributed for representative sampling. The area within the burn was extracted using the burn perimeter, and the population of pixels within the burn was summarized for both sensors (Table 1). Cloud effects appeared in the $dNBR_{ETM+}$, but cloud shadow and surface areas generally fell outside the perimeter. A slight effect of the Hoover fire in progress appeared in the pre-fire AVIRIS dataset when the fire was still very small after burning for 21 days. The $dNBR_{AVIRIS}$ showed the hot areas as dark spots in the extreme lower portion of the burn.

Analysis of the spectral responses confirmed the selection of channels 47 and 210 for detecting burn severity. Within the high severity burn plots, the mean difference between pre- and post-fire spectra at channel 47 was 0.14 with a standard deviation of 0.18 (Table 2). Channel 210 showed a larger absolute difference with a mean of 0.22 and a standard deviation of 0.06. Mean differences decreased as severity decreased in the moderate severity, low severity, and unburned plots.

Fig. 7 shows a typical response of AVIRIS channels 47 and 60 at wavelengths of 788 and 913 nm. Post-fire reflectance values decreased the most on average at those wavelengths, indicating a near complete loss of living vegetation. Channel 210 at 2370 nm showed the greatest positive response on average. Fire increased reflectance the most at that wavelength over the entire measured spectral range. This response is primarily the result of near complete canopy combustion, exposed ash and bare soil, and charred

Table 1
Descriptive statistics for within-burn $dNBR_{ETM+}$ compared to $dNBR_{AVIRIS}$

	$dNBR_{ETM+}$	$dNBR_{AVIRIS}$
Mean	167	11
S.D.	182	231
Median	115	−36
Mode	56	−89
Skewness	1.5	1.2
Kurtosis	2.7	1.7
Minimum	−491	−1125
Maximum	1026	1171
Pixels	32899	146455

Table 2
Mean and standard deviations for difference in spectra between pre- and post-fire at channels 47 and 210 for plots at each of the burn severity levels

Severity level	Number of plots	Channel 47		Channel 210	
		Mean	S.D.	Mean	S.D.
		Reflectance			
High	16	0.14	0.18	− 0.22	0.06
Moderate	26	0.05	0.02	− 0.12	0.06
Low	11	− 0.02	0.04	− 0.07	0.00
Unburned	10	− 0.03	0.04	− 0.04	0.01

large logs (Fig. 2). Furthermore, channel 210 at 2370 nm exhibited the greatest variation in spectral response, suggesting potentially high information content for fire severity. Channel 148 at 1762 nm also had fairly high positive change due to fire; however, the variation in that channel throughout the burn was considerably less than channel 210 at 2370 nm. The implication was that dynamic association of spectral responses at 788 or 913 nm and 2370 nm should provide significant statistical leverage for distinguishing degrees of burn severity on the ground.

The moderate burn severity comparison (Fig. 8) shows close to the same separation of reflectance values in the short wavelength infrared (1500–2500 nm), but presence of a small amount of green vegetation is indicated by a slight "red-edge" response at 700 nm. In addition, the exposure of dead needles and branches was indicated by absorption in the ligno-cellulose bands (Elvidge, 1990).

The low burn severity comparison (Fig. 9) shows very similar reflective response as the moderately burned area in both the near infrared and short wave infrared portions of the spectrum (750–2350 nm), but there is a subtle decrease in chlorophyll absorption visible in the 550–700 nm range. The unburned comparison (Fig. 10), as expected, looks nearly the same in both years. A slight difference in chlorophyll absorption and a tapering of the red edge on the 2001 image appear to be in the normal range of variation for vegetation (Lillesand & Kiefer, 1979) and the apparent lower plant vigor compared to 2002 could be due to any combination of environmental variables or stressors, including moisture stress (Dawson & Curran, 1998; Jayaraman & Srivastava, 2002). As can be seen by comparing Figs. 7–10, burn severity levels can be separated based on the response of the AVIRIS bands.

These results fit well with results reported for fire severity detection using Landsat TM and ETM+ sensors. AVIRIS channels 47 and 60 occur within and adjacent to Landsat TM bandwidth 4 (750–900 nm) and AVIRIS channel 210 at 2370 nm occurs at the long wavelength edge of Landsat TM bandwidth 7 (2090–2350 nm). The latter band reflectances have been shown to respond most dramatically to burning among Landsat bandwidths (Morath & Rockwell, 2002). Similar reasoning should be applicable to the 913 and 1762 nm AVIRIS channels with regard to their effectiveness for discriminating burn severity.

We validated the severity analysis by comparing Composite Burn Indices (CBI) from 63 field plots with dNBR values for both the ETM+ and AVIRIS imagery (Key & Benson, 2002). For ETM+ data, the regression of CBI as a

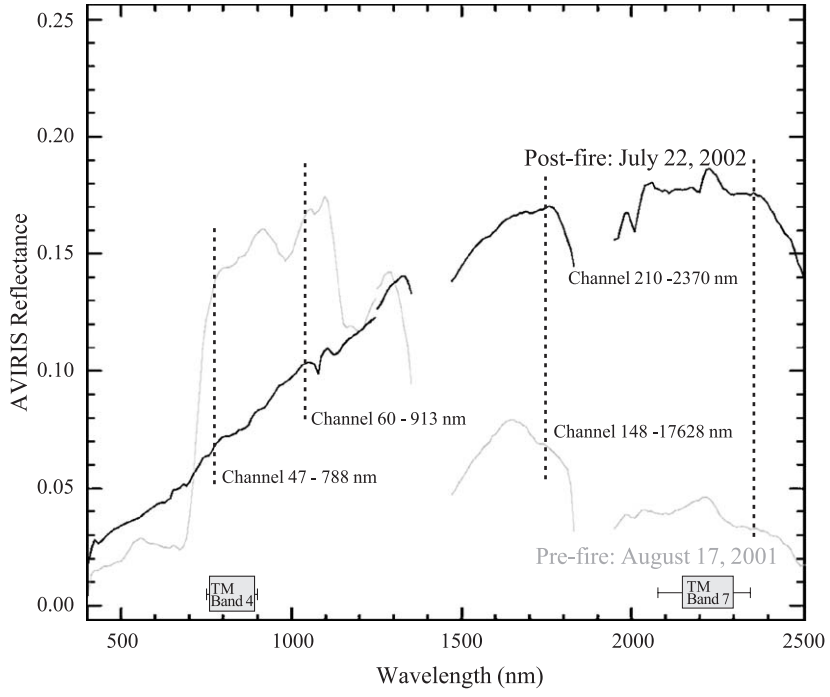

Fig. 7. Pre- and post-fire AVIRIS spectra—high severity area. Channels 47 and 60 at wavelengths 788 and 913 nm showed the greatest negative response to fire, while channels 210 and 2370 showed the greatest positive response.

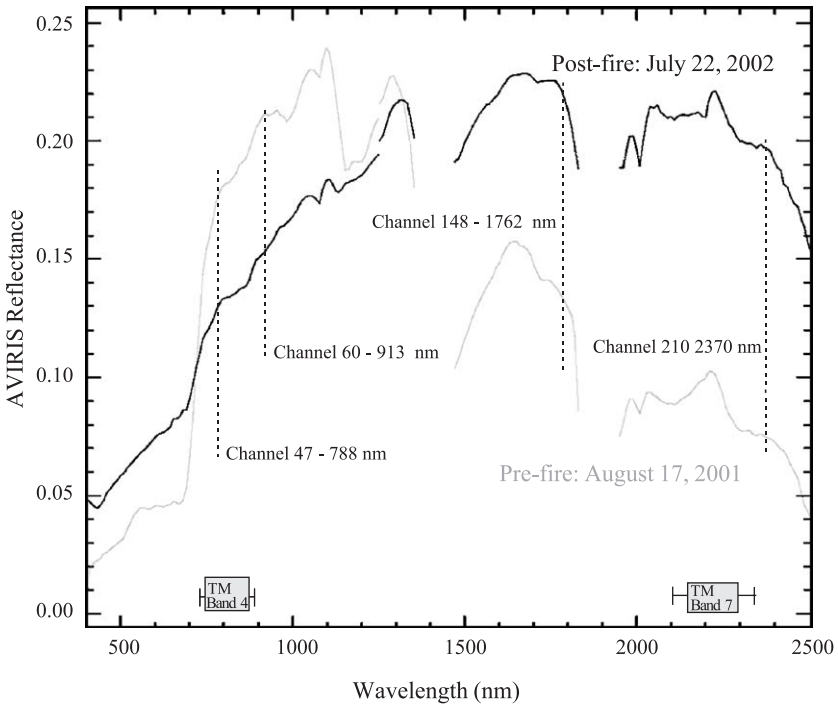

Fig. 8. Pre- and post-fire AVIRIS spectra—moderate severity area. The moderate severity area shows close to the same separation of reflectance values in the short wavelength infrared (1500–2500 nm) as the high severity area, but the presence of a small amount of green vegetation is indicated by the "red edge" response at 700 nm.

function of dNBR is shown in Fig. 11. A second-order polynomial provides a good fit for the data with an asymptote at approximately dNBR = 750. The regression for the dNBR using AVIRIS data as a function of CBI is shown in Fig. 12. In this case, the asymptote also occurs at about dNBR = 750. Both regressions have high R^2 values

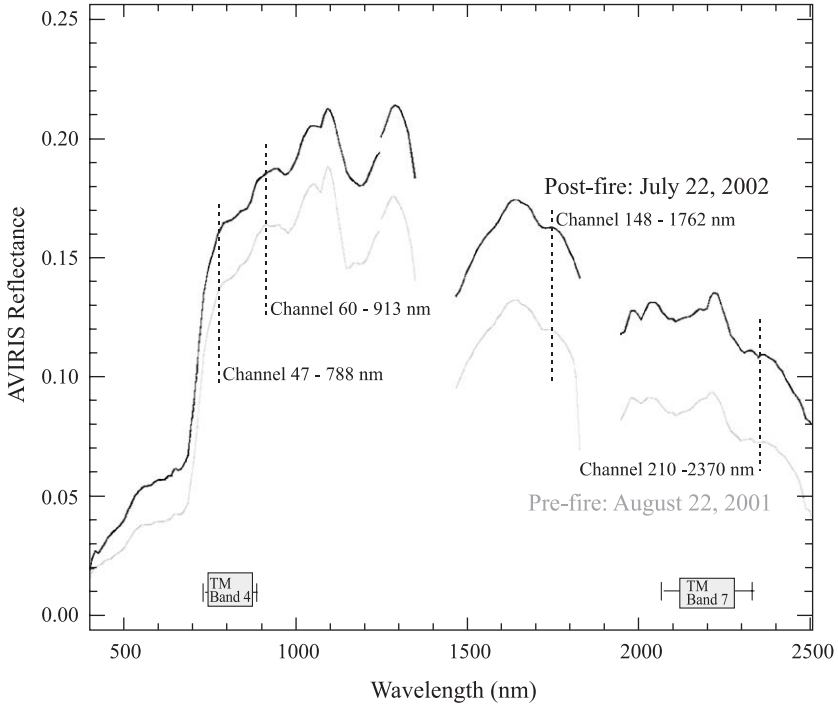

Fig. 9. Pre- and post-fire AVIRIS spectra—low severity area. The low severity area shows a similar response as the moderate severity area in both the near infrared and short wave infrared portions of the spectrum (750–2350 nm), but a subtle decrease in absorption by chlorophyll is visible in the 550–700 nm range.

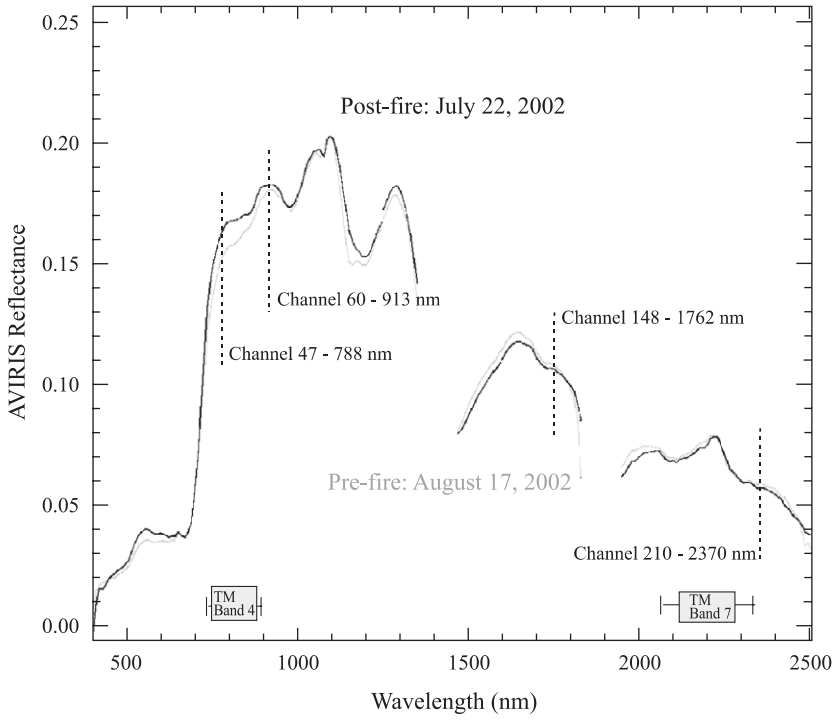

Fig. 10. Pre- and post-fire AVIRIS spectra—unburned area. This area appears similar in both years. A slight difference in chlorophyll absorption and a tapering of the red edge on the 2001 images suggests that vegetation was slightly drier or less vigorous in 2001 compared to 2002.

and are nearly similar, with only a 0.04 difference in unexplained variance.

5. Discussion

Changes in reflectance exhibited by both ETM+ and AVIRIS datasets used in this study were the result of the fire occurring between pre- and post-fire acquisitions. No other possible causes could explain the magnitude of change exhibited within the burn perimeter given the phenological matching of pre- and post-fire data and the relatively short 1-year period separating acquisitions. Moreover, the burn occurred within a national park where no other disturbances occurred during the sampling interval. The strong responses across several portions of the spectrum indicate the per channel information content potential for burn severity is high. As expected, unburned forest pixels within the perimeter of the burn reinforced that notion because they did not show much change in reflectance spectra pre- to post-fire (Fig. 10).

Though AVIRIS datasets are most frequently used in single-date classification of surface materials (Kokaly,

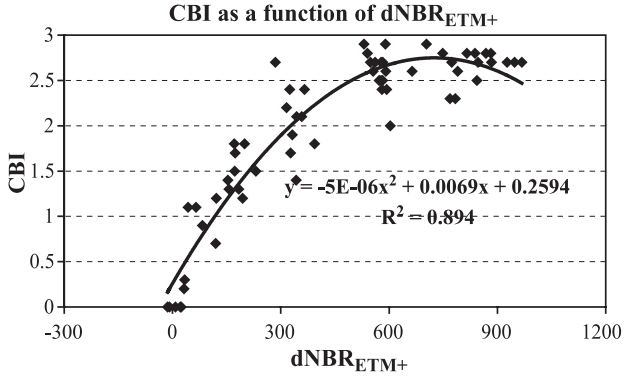

Fig. 11. Regression of the Composite Burn Index as a function of the differenced Normalized Burn Ratio based on ETM+ data using a second order polynomial. The r^2 was 0.894 and the CBI reached a maximum at about dNBR = 750.

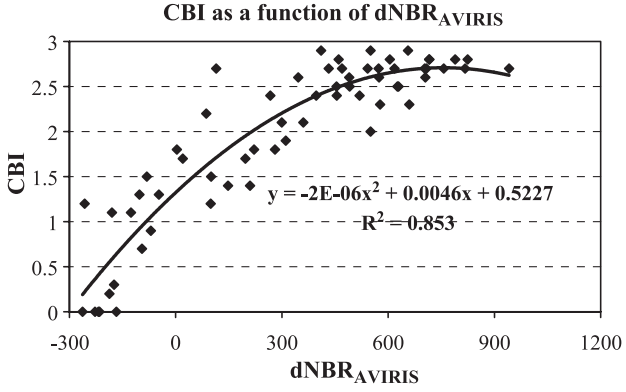

Fig. 12. Regression of the Composite Burn Index as a function of the differenced Normalized Burn Ratio based on AVIRIS data using a second order polynomial. The r^2 of 0.853 was slightly less than for the regression using ETM+ data but the maximum CBI was similar.

2002), the availability of two datasets bracketing a wildland fire allowed us to compare and validate multi-temporal differencing techniques routinely applied to wildland fires using Landsat ETM+ data. Given the much greater spectral resolution of AVIRIS, we were interested in whether the ETM+ was sampling the most burn-responsive portions of the spectrum, or whether AVIRIS revealed other more responsive portions (i.e. bandwidths), which were not sampled by ETM+. In the latter case, one could conclude that ETM+ was not optimally sampling for burn severity. Furthermore, the near-continuous sampling of AVIRIS channels across the spectrum allowed us to examine in detail whether assumptions about ETM+ bandwidths were really valid, vis-à-vis band 4 reflectance decreases the most post-fire while band 7 reflectance increases the most. Understanding such radiometric behavior is key to applying the correct bandwidths for optimal resolution of burn severity.

The fact that two AVIRIS channels with greatest combined response fell within or very close to the ETM+ sensor bandwidths having the most sensitivity to fire effects suggested that ETM+ bands 4 and 7 were actually capturing very dynamic bandwidths reacting to fire. Moreover, the AVIRIS response was high across all channels comprising ETM+ bands 4 and 7, so those entire bandwidths appeared relevant to detecting severity. In addition, different combinations of AVIRIS channels within those bandwidths would likely provide good severity detection capability. AVIRIS independently confirmed earlier assumptions about bandwidth relationships to fire and gave added support for the use of ETM+ bands 4 and 7 to quantify burned area.

We did not fully address whether some other set of AVIRIS channels may do a better job at discriminating fire effects than ETM+. However, evidence in Figs. 7–10 suggests that other spectral regions sampled by AVIRIS, e.g. in the vicinity of channels 60 and 148, would have good potential for quantifying burns. However, those regions do not appear to exhibit any greater response than the ETM+ band 4 and 7 regions, at least in regard to detection capability. We did not explore relationships of these channels to actual surface materials because of our objective of comparing AVIRIS to ETM+ in the context of change detection. However, the materials discrimination power of AVIRIS would be one area for further study that would likely expand its utility for burn severity discrimination, over and beyond that of ETM+.

We used the dNBR as a radiometric index to relate to burn severity. The NBR was designed to enhance the variable ETM+ band 4 and 7 responses to fire by normalizing their difference, which compensates for variation in overall brightness within the scene, such as between light and dark aspects. Since the two bandwidths exhibit high and opposite responses to fire effects, the NBR should accentuate those effects over and beyond other band combinations. When the change in NBR is calculated pre- to post-fire, the dNBR provides a scale of change in the index, as well as separation of burned area from unburned. In the temporal difference, unburned retains dNBR values near zero, signifying very little or no change. If severity is considered as the degree of ecological change resulting from fire, a fire-bracketing temporal change in the NBR should represent burn severity.

Although it could be argued that the higher spectral resolution of AVIRIS could produce better correlations with burn severity than the broader bandwidths of ETM+, the results were mixed. The sample of field plots exhibited a greater range of $dNBR_{AVIRIS}$ compared to $dNBR_{ETM+}$ (dNBR −26 to 1020 vs. −302 to 979, respectively), suggesting possibly that $dNBR_{AVIRIS}$ has more sensitivity to fire effects. On the other hand, the correlation of dNBR with plot CBI values was high but nearly identical between the sensors (Figs. 11 and 12). Both showed good association across the range of burn severity. One reason for the similarity may be the CBI used to measure severity on the ground. Since the CBI aggregates many effects over multiple strata of the site and uses a relatively large plot size, the generalized interpretation obtained from CBI may not be adequate in its applied form to fully exploit the detail obtained from AVIRIS. The CBI appeared to yield similar results across the scale and resolution differences of the sensors, but a more detailed ground measure of severity may elucidate differences between AVIRIS and ETM+.

Extrapolation of these results to other fires and other ecosystems should be done with caution given the availability of just this one study where AVIRIS data bracketed a wildland fire. Because the NBR is normalized and the change measured by dNBR is relative to the status of NBR in the pre-fire scene, however; we believe that repeated comparison of AVIRIS and ETM+ spectral response would yield similar results in generally forested burns from other areas.

Timing of acquisitions does make a difference generally in the comparability of pre- and post-fire datasets. As the phenology of vegetation changes and as moisture content changes throughout a growing season, the NBR would register that in the relationship of near infrared wavelengths to shortwave infrared wavelengths. Moister and lusher conditions, for example, result in higher NBR values compared to drier and less productive states when vegetation has senesced. The dNBR, therefore, needs to be reasonably paired by phenology and moisture between the two dates, pre- and post-fire. In our case, the ETM + scenes collected on July 27, 2000, and August 2, 2002, were closely matched in terms of phenology and moisture. There were similar amounts of greenness in unburned vegetation, and the dNBR values in unburned vegetation were narrowly distributed around zero. Possibly, dates of pre- and post-fire acquisitions explain some of the slightly less correlation with AVIRIS. As indicated in Fig. 10, August 17, 2001, the date of the pre-fire image was drier and less productive overall than July 22, 2002, the post-fire image date. Drier conditions could also explain the negative shift in $dNBR_{AVIRIS}$.

An obvious benefit to burn assessment from AVIRIS is improved spatial resolution, depending on aircraft altitude. Even in our case, AVIRIS nominal resolution of 17 m represents a 3.1 times improvement over Landsat 30-m resolution. While we did not test spatial variables in comparing Landsat with AVIRIS, it was visually apparent from the images that AVIRIS provided finer spatial detail than Landsat. The increased detail suggested potential for sub stand-level measurements and more precise geo-location of ground sample points within the image. It also may facilitate burn assessments that are done in highly fragmented landscapes, such as at higher elevations or where vegetation is patchy and dispersed among bedrock outcroppings.

6. Conclusion

Based on general remote sensing principles and the logic of variable spectral responses to fire, dNBR from both sensors should produce useful results in quantifying burn severity. The capability of AVIRIS has not been thoroughly tested, however, and there remains potential for it to produce optimal results using some other spectral algorithm and a different approach to the ground measure of severity. Neither has AVIRIS been tested on a sufficient number of different fires or on fires in an adequate number of different ecosystems. Further, we believe the full capability of AVIRIS has only begun to be explored by this study. Our study does illustrate that fundamental similarities in burn severity detection capabilities exist between AVIRIS and ETM+, and that a change detection approach is informative.

Unfortunately, use of AVIRIS in multi-temporal differencing may be limited by the complexity of mission planning and the high cost of data acquisition. Moreover, AVIRIS is not continuously flown and coverage is not geographically contiguous. There are also issues of complexity in the georectification necessary for temporal differencing, especially with multiple flight lines, and terrain exhibiting high topographic relief. Some large, socioeconomically important burns may continue to attract AVIRIS overflights, but, of those, a smaller number still are likely to have comparable pre-fire data available to represent appropriate timing for the post-fire data. Until orbital imaging spectrometers with the capability of capturing data at regular intervals are in routine use, it is doubtful such data are currently practical for making burn assessments. On the other hand, most AVIRIS data acquisitions are eventually archived for access by users other than initial principal investigators. It is possible that the newly launched EO1 satellite with its hyperspectral HYPERION sensor might prove economical for providing seamless coverages necessary for pre- and post-fire evaluations.

Nonetheless, such opportunities should be explored with past AVIRIS datasets, and new pre- and post-fire hyperspectral datasets should be considered when research or management objectives justify. That may be the case, for example, when there is a need to learn from relatively large prescribed burns or to develop mechanistic models ultimately intended for more routine applications. Such approaches apply knowledge gained in great detail about cause and effect to algorithms implemented at coarser resolutions.

Acknowledgements

The authors thank the Joint Fire Science program for funding this study. We would also like to thank Kara Paintner and Mark Grupé of the National Park Service in Yosemite National Park for supervising field data collection and database construction; Ian McCubbin of the National Atmospheric and Space Agency for arranging the AVIRIS flights; Joe Boardman of Analytical Imaging and Geophysics for georectifying the images; and Susan Ustin and Carlos Ramirez of the University of California, Davis, for assisting with the analysis of the AVIRIS data.

References

Boles, S. H., & Verbyla, D. L. (1999). Effect of scan angle on AVHRR fire detection accuracy in interior Alaska. *International Journal of Remote Sensing*, *20*, 3437–3443.

Bourgeau-Chaves, L. L., Kasischke, E. S., Tuckman, M., & Mudd, J. P. (2002). Mapping fire scars in global boreal forests using imaging radar data. *International Journal of Remote Sensing*, *23*, 831–837.

Chuvieco, E. (1999). Measuring changes in landscape pattern from satellite images: Short-term effects of fire on spatial diversity. *International Journal of Remote Sensing*, *22*, 2331–2346.

Dawson, T. P., & Curran, P. J. (1998). Technical note: A new technique for interpolating the reflectance red edge position. *International Journal of Remote Sensing*, *19*, 2133–2139.

Diaz-Delgado, R., Lloret, F., & Pons, X. (2003). Influence of fire severity on plant regeneration by means of remote sensing imagery. *International Journal of Remote Sensing*, *24*, 1751–1763.

Elvidge, C. D. (1990). Visible and near infrared reflectance characteristics of dry plant materials. *International Journal of Remote Sensing*, *11*, 1775–1795.

Eva, H., & Lambin, E. F. (1998). Burnt area mapping in central Africa using ASTR data. *International Journal of Remote Sensing*, *19*, 3473–3497.

Gao, B. C. (1996). A normalized difference water index for remote sensing of vegetation liquid water from space. *Remote Sensing of Environment*, *58*, 257–266.

Green, R. O., Eastwood, M. L., Sarture, C. M., Chrien, T. G., Aronsson, M., Chippendale, B. J., Faust, J. A., Pavri, B. E., Chovit, C. J., Solis, M., & Williams, O. (1998). Imaging spectroscopy and the Airborne Visible/Infrared Imaging Spectrometer (AVIRIS). *Remote Sensing of Environment*, *65*, 227–248.

Hlavka, C. A., Ambrosia, V. G., Brass, J. A., Rezendez, A. R., & Guild, L. S. (1996). Mapping fire scars in the Brazilian Cerrado using AVHRR imagery. In J. S. Levine (Ed.), *Biomass Burning and Global Change, vol. 2* (pp. 555–560). Cambridge: MIT Press.

Hunt, E. R., & Rock, B. N. (1989). Detection of changes in leaf water content using near and middle-infrared reflectances. *Remote Sensing of Environment*, *30*, 43–54.

Jayaraman, V., & Srivastava, S. K. (2002). The invariance of res-edge

inflection wavelengths derived from ground based spectro-radiometer and space-borne IRS-P3: MOS-B data. *International Journal of Remote Sensing*, *23*, 2741–2765.

Kasischke, E. S., & French, H. F. (1995). Locating and estimating the areal extent of wildfires in Alaskan boreal forests using multiple-season AVHRR NDVI composite data. *Remote Sensing of Environment*, *51*, 263–275.

Key, C., Benson, N., Sorbel, B., Zhu, Z., Ohlen, D., Howard, S., & Clement, B. (2002). *National Park Service-U.S. Geological Survey National Burn Severity Mapping Project.* Retrieved September 30, 2002 from USGS EROS Data Center archive and web site: http://edc2.usgs.gov/fsp/severity/fire_main.asp.

Key, C. H., & Benson, N. C. (1999). Measuring and remote sensing of burn severity. In L. F. Neuenschwander, & K. C. Ryan (Eds.), *Proceedings Joint Fire Science Conference and Workshop, vol. II* (p. 284). Moscow, ID: University of Idaho and International Association of Wildland Fire.

Key, C. H., & Benson, N. C. (2002). Remote sensing measure of severity, the normalized burn ratio. *Fire effects monitoring and inventory protocol, Landscape Assessment.* Retrieved March 30, 2003 from Systems for Environmental Management and USDA Fire Sciences Laboratory, Rocky Mountain Research Station Web site: http://www.fire.org/firemon/lc.htm.

Key, C. H., & Benson, N. C. (2004). Ground Measure of Severity, The Composite Burn Index. In D. C. Lutes, R. E. Keane, J. F. Caratti, C. H. Key, N. C. Benson, & L. J. Gangi (Eds.), *FIREMON: Fire Effects Monitoring and Inventory System*. Gen. Tech Rep. RMRS-GTR-XXX, Ogden, UT: U.S. Department of Agriculture, Forest Service, Rocky Mountain Research Station. XX p.

Kokaly, R. F. (2002). Application of airborne imaging spectroscopy to areas impacted by wildfires. In J. L. Colbert, & R. K. Livingston (Eds.), *Second U.S. Geological Survey Wildland Fire Workshop*, (p. 59). US Geological Survey, Denver, CO, USA. USGS Open File Report 02-11.

Koutsias, N., Karteris, M., Fenandez-Palacios, A., Navarro, C., Jurado, J., Navarro, R., & Lobo, A. (1999). Burnt land mapping at local scale. In E. Chuvieco (Ed.), *Remote sensing of large wildfires in the European Mediterranean basin* (pp. 159–187). Berlin: Springer-Verlag.

Kushlaw, J. D., & Ripple, W. J. (1998). Assessing wildfire effects with Landsat thematic mapper data. *International Journal of Remote Sensing*, *19*, 2493–2507.

Li, Z., Nadon, S., Cihlar, J., & Stocks, B. (2000). Satellite-based mapping of Canadian boreal forest fires: Evaluation and comparison of algorithms. *International Journal of Remote Sensing*, *21*, 3071–3082.

Lillesand, T., & Kiefer, R. (1979). *Remote sensing and image interpretation*. New York: Wiley & Sons. 612 pp.

Lutes, D. C., Keane, R. E., Caratti, J. F., Key, C. H., Benson, N. C., & Gangi, L. J. (2004). FIREMON: Fire Effects Monitoring and Inventory System. Gen. Tech Rep. RMRS-GTR-XXX, Ogden, UT: U.S. Department of Agriculture, Forest Service, Rocky Mountain Research Station. In press.

Markham, B. L. & Barker, J. L. (1986). Landsat MSS and TM post-calibration dynamic ranges, exoatmospheric reflectances and at-satellite temperatures. *EOSAT Landsat Technical Notes,* 1, 3–8.

Miller, J. D., & Yool, S. R. (2002). Mapping forest post-fire canopy consumption in several overstory types using multi-temporal Landsat TM and ETM data. *Remote Sensing of Environment*, *82*, 481–496.

Morath, L., Rockwell, R. F., Kokaly, R. F., Root, R. R., & Goodman, S. (2002). Post-fire characterization of the land surface and vegetation using imaging spectroscopy data for Cerro Grande NM and Left Hand Creek WY. *Geological Society Abstracts with Programs*, *34*, 552.

National Wildfire Coordinating Group. (1996). *Glossary of wildland fire terms*. Boise ID, USA: National Interagency Fire Center. Pub. PMS 205/NFES 1832. 141 pp.

Patterson, M. W., & Yool, S. R. (1998). Mapping fire-induced vegetation mortality using Landsat Thematic Mapper data: A comparison of linear transformation techniques. *Remote Sensing of Environment*, *65*, 132–142.

Perez, B., & Moreno, J. M. (1998). Methods for quantifying fire severity in shrubland-fires. *Plant Ecology*, *139*, 91–101.

Riano, D., Chuvieco, E., Ustin, S., Zomer, R., Dennison, P., Roberts, D., & Salas, J. (2002). Assessment of vegetation regeneration post-fire through multitemporall analysis of AVIRIS images in the Santa Monica Mountains. *Remote Sensing of Environment*, *79*, 60–71.

Roberts, D. A., Gardner, M., Church, R., Ustin, S., Scheer, G., & Green, R. O. (1998). Mapping chaparral in the Santa Monica Mountains using multiple endmenber spectral mixing. *Remote Sensing of Environment*, *65*, 267–279.

Scholes, R. J., Kendall, J., & Justice, C. O. (1996). The quantity of biomass burned in southern Africa. *Journal of Geophysical Research-Atmospheres*, *10*(D19), 23667–23676.

Siegert, F., & Ruecker, G. (2000). Use of multitemporal ERS-2 SAR images for identification of burned areas in south-east Asian rainforest. *International Journal of Remote Sensing*, *21*, 831–837.

Stroppiana, D., Pinnock, S., Pereira, J. M. C., & Gregoire, J. -M. (2002). Radiometric analysis of SPOT-VEGETATION images for burned area detection in Northern Australia. *Remote Sensing of Environment*, *82*, 21–37.

van Wagtendonk, J. W., van Wagtendonk, K. A., Meyer, J. B., & Paintner, K. J. (2002). The use of geographic information for fire management planning in Yosemite National Park. *George Wright Forum*, *19*, 19–39.

White, J. D., Ryan, K. C., Key, C. C., & Running, S. W. (1996). Remote sensing of forest fire severity and vegetation recovery. *International Journal of Wildland Fire*, *6*, 125–136.